Hindawi
International Journal of Aerospace Engineering
Volume 2019, Article ID 3729480, 10 pages
https://doi.org/10.1155/2019/3729480

Research Article

Analyzing the Departure Runway Capacity Effects of Integrating Optimized Continuous Climb Operations

Manuel Villegas Díaz,[1] **Fernando Gómez Comendador**,[1] **Javier García-Heras Carretero**,[2] **and Rosa María Arnaldo Valdés**[1]

[1]*Universidad Politécnica de Madrid, Madrid 28040, Spain*
[2]*Universidad Carlos III de Madrid, Leganés 28911, Spain*

Correspondence should be addressed to Manuel Villegas Díaz; manuel.villegas.diaz@alumnos.upm.es

Received 30 August 2018; Revised 18 December 2018; Accepted 25 December 2018; Published 11 February 2019

Guest Editor: Yoshinori Matsuno

Performing Continuous Climb Operation (CCO) procedures enable the reduction of the environmental footprint and the improvement of the trajectory efficiency when individually operated. However, its operation may affect negatively the overall operational efficiency at Terminal Manoeuvring Areas (TMAs). The estimation of capacity is a matter of paramount importance to all airport planning and analyzing the capacity effects of this particular operational technique on a certain scenario will definitely help on evaluating its potential applicability. In this paper, departure runway capacity at the Adolfo Suárez Madrid-Barajas airport was operationally evaluated when introducing CCOs. The considered trajectories consisted of multiobjective optimized CCOs based on the optimal control theory, using the pseudospectral direct numerical method. These scenarios allowed addressing of the incremental variations of CCOs versus conventional departures, through fast time simulation, with the objective to assess the effects on the operations.

1. Introduction

Defined as an uninterrupted climb flight operation allowing the aircraft to attain initial cruise flight level at an optimum air speed with optimal thrust settings [1], the Continuous Climb Operation (CCO) leads to a significant fuel economy and environmental benefits. The improvement of flight trajectories through the execution of a flight profile optimized to the performance of an aircraft represents a significant enabler for Trajectory-Based Operations (TBO), which is one of the four pillars (four-phase improvement) defined on Single European Sky ATM Research (SESAR) [2].

At a local level, continuous operating techniques, such as CCOs, can significantly reduce the environmental footprint in living areas around the airports. Besides, this technique allows the airspace users to plan and, ideally, to fly a trajectory which will be closer to their preferences whilst complying with operational constraints. This may be translated into positive contributions on cost benefits through satisfying the airspace users' business needs.

As part of the Aviation System Block Upgrade (ASBU) system engineering modernization strategy, Global Air Navigation Plan (GANP) [3], the International Civil Aviation Organization (ICAO) prioritizes the usage of CCOs among other initiatives. Along these lines, global air navigation initiatives for future air traffic management like the Single European Sky ATM Research (SESAR) [2] in Europe and The Next Generation Air Transportation System (NextGen) [4] in the United States of America put in place innovative activities for the optimization of vertical trajectories. The departure phase of the flight has been identified as a key area where substantial environmental benefits could be achieved.

The optimization of flight trajectories for terminal operating procedures has been a problem extensively tackled for years, particularly focused on arrival procedures. Limited research has been conducted in terms of "pure" CCOs, as the benefits did not seem to be noteworthy. However,

considering that engines usually run close to full throttle during a climb phase, there exist the potential for reducing the environmental footprint in living areas around the airports. In this regard, McConnachie et al. [5] presented the evidences for environmental performance change in case CCOs are applied at certain airports. Nevertheless, it was plausibly assumed that a CCO is just an uninterrupted climb. The successful application of a CCO should not be simplistically reduced to the operation of an uninterrupted climb procedure, which implies inexistent level-off segments. It is important to note the importance of factors like the aircraft, airport type, aircraft weight, runway, Standard Instrument Departure (SID), and operational constraints when identifying the CCO profile optimized to the performance of the aircraft.

However, the integration of a CCO-operating technique in a Terminal Manoeuvring Area (TMA) requires the analysis of one of the most important parameters on airport planning, which is capacity. This Key Performance Area (KPA), which is one of the eleven KPAs defined by ICAO, at high-density terminal areas motivated the interesting work presented by Li et al. [6]. The model introduced for terminal area design is mainly focused on arrival trajectories. It is important to highlight that the integration of a pure CCO has not been directly considered by recent investigations; therefore, an assessment of the operational limitations and its potential effects would be tempting.

In Europe, SESAR targets up to 30% reduction in departure delays. On the other hand, its environmental expectation targets up to 10% reduction in CO_2 emissions including a positive impact on noise and air quality. Along with this KPA, the operational efficiency aims up to 6% reduction in flight time and up to 10% reduction in fuel burn. The successful achievement of all these targets is not trivial considering that the implementation of an environmental friendly operational procedure may produce negative effects on other KPAs.

It is likely to obtain local positive environmental effects through the application of optimized CCOs whilst affecting negatively airport efficiency operations. In other words, a new operating technique that seems to be beneficial when it is applied in isolation may not be quite beneficial when integrated as a part of a complete scenario. The study presented at this paper is aimed at studying the capacity effects when applying optimized CCOs. The Adolfo Suárez Madrid-Barajas airport (ICAO code, LEMD) has been selected as the test scenario to evaluate the effects on capacity when facilitating CCOs. The study has been enabled by a consolidated multiobjective software model, which was previously developed by the authors, for the computation of aircraft trajectories when performing optimal CCOs in terms of noise and fuel consumption.

To this end, the paper is organized as follows: Section 2 gathers the description of the scenario. Section 3 includes the aircraft performance model. Section 4 provides the operational constraints as well as the boundary conditions. Section 5 describes the used methodology for tackling the exercise. Section 6 presents the results, which offers the main findings of the analysis. And finally, Section 7 concludes with the key remarks of the study.

2. Departures at Adolfo Suárez Madrid-Barajas

Adolfo Suárez Madrid-Barajas is the largest airport in Spain with 378,566 total operations in 2017. Considered as one of the largest airport in Europe by physical size, it is the country's busiest airport in Spain, and Europe's sixth busiest. The airport is predominantly operated in north configuration and runway (RWY) 36L was selected as the preferred option for this study. In particular, the chosen flight segments go from ground to waypoint (WPT) AVILA. A shorter flight segment which is common for two Standard Instrument Departures (SIDs): Bardi Two Tango (BARDI2T) and Cáceres One Tango (CCS1T), and a longer flight segment, which is shared by Bardi Two Kilo (BARDI2K) SID and Cáceres One Kilo (CCS1K) SID. The operations of these SIDs are limited by the performance of the aircraft and aircraft type as clarified below.

Figure 1 shows a zoom view of the published chart, which includes the SIDs for RWY 36L, usable at daytime. SIDs BARDI2T/CCS1T are only allowed to authorized aircraft and, thus, BARDI2K/CCS1K becomes mandatory to listed aircraft due to noise restrictions. Published noise abatement procedures are applicable to all takeoffs, unless exceptionally cancelled due to an event that cannot be reasonably anticipated.

This is a challenging scenario as the performance of the aircraft plays a relevant role when performing BARDI2K/CCS1K or BARDI2T/CCS1T SID. The facilitation of CCO when performing these departure segments must satisfy the airspace restrictions and operational constraints.

3. Aircraft Performance

This section gathers the aircraft dynamics equations considered for this study. The considered representation of the aircraft is a dynamic model, which represents the point variable mass motion over a spherical flat nonrotating earth model besides neglecting wind components. The resulting set of differential equations of the aircraft is the following:

$$\begin{aligned}
\dot{x} &= V.\cos(\gamma),\\
\dot{h} &= V.\sin(\gamma),\\
\dot{V} &= \frac{T(h,V) - D(h,V,C_d) - m.g.\sin(\gamma)}{m(t)},\\
\dot{\gamma} &= \frac{L(h,V,C_l) - m.g.\sin(\gamma)}{m(t).V(t)},\\
\dot{m} &= -T(h,V).\eta(h,V),
\end{aligned} \tag{1}$$

where the state vector is comprised of the true airspeed V, the longitudinal position x, the aerodynamic flight path angle γ, the altitude h, and the mass of the aircraft m. In addition to the states, there are other components like T, which represents the thrust, g the gravity acceleration (assumed as a constant value), D is the aerodynamic drag, and η is the thrust-specific fuel flow.

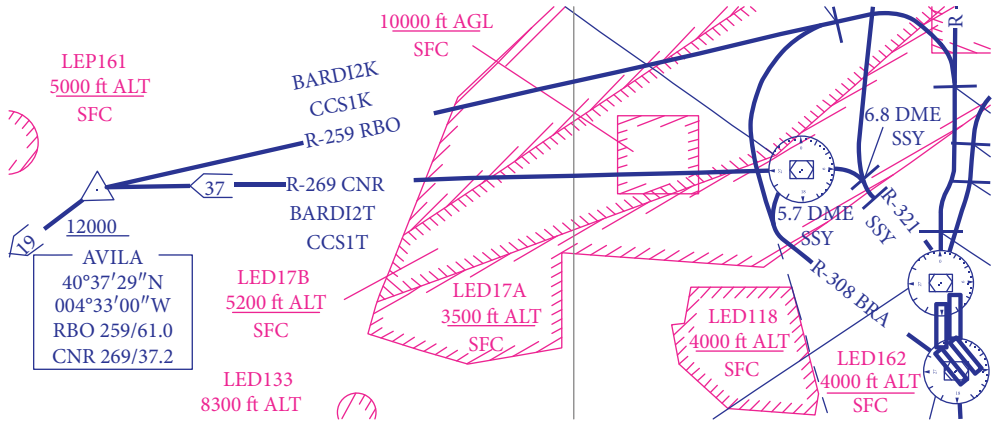

Figure 1: SIDs RWY 36L. Detailed view of selected flight segments associated to BARDI2T/CCS1T & BARDI2K/CCS1K SIDs.

Table 1: Operational constraints.

SID	BARDI2T/CCS1T	BARDI2K/CCS1K
MCG	6.4% to 10000 ft	7.5% to 4500 ft
KIAS constraints (1)	5.7 DME SSY: 180-240 kt	15 DME BRA h ≥ 6500 ft
KIAS constraints (2)	h ≤ 10000 ft KIAS ≤ 250 kt	
AVILA (2)	h ≥ 12000 ft	

In terms of the atmosphere, it has been considered the ICAO Standard Atmosphere (ISA) model [7], which presents pressure $p(h)$, density $\rho(h)$, and temperature $\tau(h)$. This model denotes p_0, ρ_0, and τ_0 for the standard values at sea level for pressure, density, and temperature, respectively.

4. Operational Constraints and Boundary Conditions

The studied scenario corresponds to RWY 36L at the Adolfo Suárez Madrid-Barajas airport. The surveillance data has been analyzed in order to identify the operational constraints of the scenario prior to the performance of the simulations. Flows for departures and arrivals have been studied. Moreover, it has also been analyzed the potential interaction of the inbound & outbound flows against the modeled flight segment for SIDs BARDI2T/CCS1T and BARDI2K/CCS1K.

Determining the capacity effects when facilitating CCOs has been applied to the aforesaid SIDs, where the performance of the aircraft plays a significant role. The clearance for flying a CCO technique does not take the aircraft operator away from being compliant with the numerous operational constraints.

The considered flight segments start with a climb on the runway heading directly to DVOR/DME SSY and finish when crossing AVILA waypoint at 12000 ft or above. The operation of these flight segments may be influenced by aircraft performance limitations, which may be translated on negative effects depending on the selected SID. It is worth mentioning that assuming the initial Air Traffic Control (ATC) clearance of maintaining 13000 ft and requesting flight level change en route may not stop a continuous climb operation in the first instance.

The assumed separation for departures is time based. The considered value is 120 seconds between any combinations of aircraft types. Regarding the operational constraints, Table 1 gathers the operational constraints, like Minimum Climb Gradient (MCG) and Knots Indicated Airspeed (KIAS), among others.

The computational cost for finding the solution is significantly higher when the problem is applied to actual scenarios due to the mandatory compliance of actual operational constraints. The initial conditions on the studied procedure are taken at the moment the aircraft lines up for taking off. Table 2 summarizes the main boundary conditions considered when modeling the departures for the considered aircraft types, Airbus 319 (A319) and Airbus 330 (A330). The surveillance data analysis performed through additional hand-tailored MATLAB models enabled the operational assessment of departure and arrival flows as well as the calculation of some relevant parameters indicated within Table 2. The analysis of the surveillance data brings up interesting facts, for example, SID BARDI2T/CCS1T is highly operated by mediums compared to heavies. Considering this, it is not realistic to consider a medium aircraft operating BARDI2K/CCS1K SID.

5. Model

Traditionally, tactical controllers manage the aircraft within their airspace domain and provide clearances to specific altitudes based on the characteristics of the traffic in terms of complexity and airspace layout. A conventional departure trajectory, which has been vertically limited, presents several level-offs before reaching the cruise level. There is a limit to

Table 2: Boundary conditions.

SID	BARDI2T/CCS1T	BARDI2K/CCS1K
RWY (h)	0 ft	
RWY (KIAS)	0 knots	
RWY (Rate of Climb (ROC))	0 ft	
AVILA (h)	16200 ft–26400 ft	
AVILA (KIAS)	392 knots (A319)/389 knots (A330)	401 knots (A330)
AVILA (ROC)	2165 fpm (A319)/1546 fpm(A330)	1467 fpm (A330)
Flight distance	47 NM	56 NM

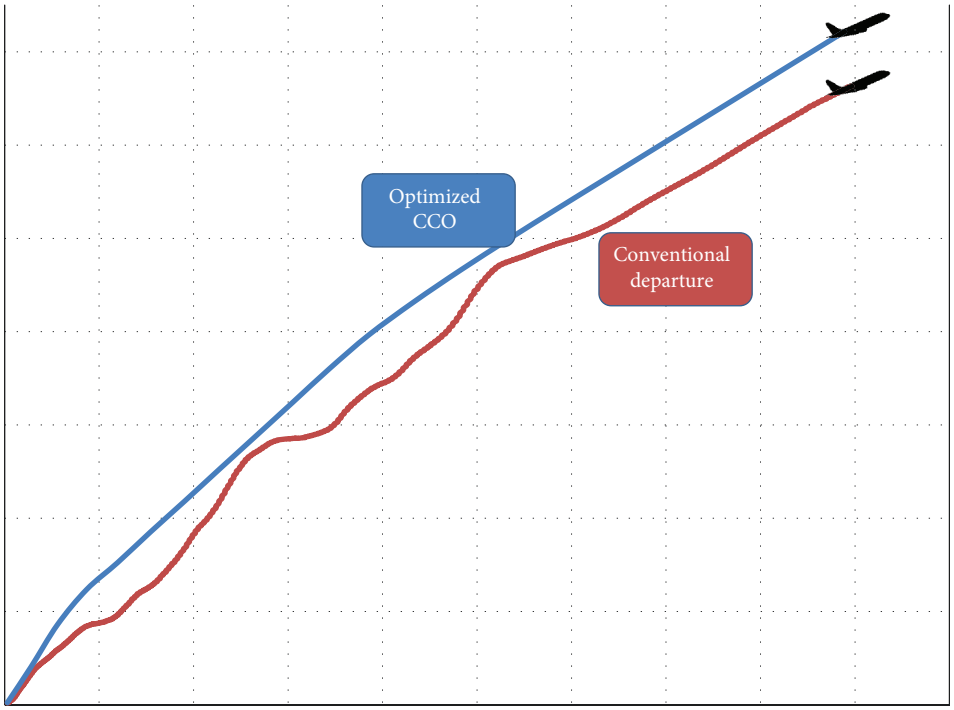

Figure 2: Departure flight paths. Optimized CCO versus standard departure.

the number of aircraft a controller can keep track of at one time, so as airspace has to be subdivided in airspace sectors, the flights require leveled segments. These leveled segments on the vertical profile penalize the aircraft efficiency and prevent the aircraft from flying its ideal trajectory. Conversely, the performance of an optimized CCO that allows the aircraft to attain initial cruise flight level at an optimum air speed with optimal thrust settings brings noteworthy benefits to the flight efficiency. Figure 2 illustrates a standard departure and an optimized CCO where the differences between the departure flight paths can be appreciated.

The mathematical method used for the optimization of the CCO is based on the optimal control theory, which aims at determining the control input that will cause a system to achieve the control objectives, whilst satisfying the constraints and also optimizing some performance criterion. The trajectory optimization problem was solved following an open loop terminal control problem that allows the constraints acting on the dynamical system to be considered in a way that the obtained trajectory will be admissible.

Commercial aircraft trajectory problems have been tackled through open loop optimal control techniques [8–10]. However, optimal control problems are characterized for being highly nonlinear, and thus, it becomes certainly difficult to find analytical solutions. Numerical methods are typically used for this purpose, and direct methods fit the approach for the trajectory optimization problem. A simplistic description of direct methods could be presented as discretizing the optimal control problem at the nodes of discretization, resulting to a NLP ready to be solved.

5.1. Optimal Control Problem. With the aim of facilitating the discussion, consider the following optimal control problem (OCP):

$$\min J(t, x(t), u(t), l) = E\left(t^{\mathrm{F}}, x\left(t^{\mathrm{F}}\right)\right) + \int_{t^{\mathrm{I}}}^{t^{\mathrm{F}}} L(x(t), u(t), l)dt, \tag{2}$$

subject to

$\dot{x}(t) = f(x(t), u(t), l)$, dynamic equations; $0 = g(x(t), u(t), l)$, algebraic equations; $x(t^{\mathrm{I}}) = x^{\mathrm{I}}$, initial boundary conditions; $\psi(x(t^{\mathrm{F}})) = 0$, terminal boundary conditions; and $\phi_l \le \phi[x(t), u(t), p] \le \phi_u$, path constraints.

Variable $t \in [t^{\mathrm{I}}, t^{\mathrm{F}}] \subset \mathbb{R}$ represents time, and $l \in \mathbb{R}^{n_l}$ is a vector of parameters. Notice that the initial time t^{I} is fixed and the final time t^{F} might be fixed or left undetermined. $x(t)$: $[t^{\mathrm{I}}, t^{\mathrm{F}}] \to \mathbb{R}^{n_x}$ represents the state variables. $u(t)$: $[t^{\mathrm{I}}, t^{\mathrm{F}}] \to \mathbb{R}^{n_u}$ represents the control functions, also referred to as control inputs, assumed to be measurable. The objective function $J : [t^{\mathrm{I}}, t^{\mathrm{F}}] \times \mathbb{R}^{n_x} \times \mathbb{R}^{n_u} \times \mathbb{R}^{n_l} \to \mathbb{R}$ is given in the Bolza form. It is expressed as the sum of the Mayer term $E(t^{\mathrm{F}}, x(t^{\mathrm{F}}))$ and the Lagrange term $\int_{t^{\mathrm{I}}}^{t^{\mathrm{F}}} L(x(t), u(t), l)dt$.

Functions $E : [t^{\mathrm{I}}, t^{\mathrm{F}}] \times \mathbb{R}^{n_x} \to \mathbb{R}$ and $L : \mathbb{R}^{n_x} \times \mathbb{R}^{n_u} \times \mathbb{R}^{n_l} \to \mathbb{R}$ are assumed to be twice differentiable. The system is a DAE system in which the right hand side function of the differential equations $f : \mathbb{R}^{n_x} \times \mathbb{R}^{n_u} \times \mathbb{R}^{n_l} \to \mathbb{R}^{n_x}$ is assumed to be piecewise Lipschitz continuous, and the derivative of the algebraic right hand side function $g : \mathbb{R}^{n_x} \times \mathbb{R}^{n_u} \times \mathbb{R}^{n_l} \to \mathbb{R}^{n_z}$ with respect to z is assumed to be regular. $x^{\mathrm{I}} \in \mathbb{R}^{n_x}$ represents the vector of initial conditions given at the initial time t^{I} and the function $\psi : \mathbb{R}^{n_x} \to \mathbb{R}^{n_q}$ provides the terminal conditions at the final time, and it is assumed to be twice differentiable. The system must satisfy algebraic path constraints given by the function $\phi : \mathbb{R}^{n_x} \times \mathbb{R}^{n_u} \times \mathbb{R}^{n_l} \to \mathbb{R}^{n_\phi}$ with lower bound $\phi_l \in \mathbb{R}^{n_\phi}$ and upper bound $\phi_u \in \mathbb{R}^{n_\phi}$. Function ϕ is assumed to be twice differentiable.

The Chebyshev pseudospectral method, which has demonstrated advantages over indirect methods, is widely used in engineering applications, especially on trajectory optimization problems [11]. This spectral method utilizes orthogonal polynomials instead of piecewise continuous polynomials when approximating state and control variables. F. Fahroo and I. M. Ross presented at [12] the demonstration of the fact that Chebyshev-Gauss-Lobatto (CGL) method yields more accurate results than those obtained from the traditional collocation method. Recently, in [13], an intensive analysis on different direct collocation methods to solve a classical problem on ATM was presented. Once again, pseudospectral collocation method has proven better results on accuracy and computational time but uncertainties in vertical trajectories during a climb/descent.

In this investigation, the operational flight paths were obtained through multiobjective optimization process based on CCO principles by a CGL pseudospectral method. The calculations were executed through a hand-tailored software tool implemented on AMPL modeling language [14] for Airbus A319 and A330 aircraft, using IPOPT as the NLP solver. The latest Base of Aircraft Data (BADA 4.1 [15]) supported the AMPL self-implemented optimization model. AMPL is an algebraic modeling system for mathematical programming of large-scale optimization problems. For the sake of clarity, a solver is defined as the number-crunching algorithm that computes optimal solutions. The calculated optimal trajectories were stored in a database for further processing.

5.2. Optimization Criteria. The environmental optimization criterion has been modeled considering two magnitudes: maximum A-weighted sound level ($L_{\max}$) and fuel burn. Aiming at supporting this multiobjective optimization, the weighted combination of the aforementioned factors has been implemented as follows:

$$J = a\,(\text{noise}) + b\,(\text{fuel consumption}), \tag{3}$$

where a and b are adjustable weighting constants. The values of these constants are directly related to the trade-off between noise exposure and fuel consumption/emissions. In this study, both factors have received the same weighting avoiding the prioritization of one of them. It is out of the scope of this study to present the analysis of Pareto for the aforesaid weighting constants. The considered parameter for noise optimization, maximum A-weighted sound level ($L_{\max}$), is based on the methodology employed by the Integrated Noise Model (INM) [16]. The core of this methodology relies on the Noise-Power-Distance (NPD).

5.3. Departure Capacity Model. The following steps were required to establish the appropriate enablers that allow addressing of the main objective of this study, in other words, the means of evaluating the operational implications of integrating optimal CCOs.

The scenario was modeled considering operational and physical constraints. The derivation of the runway utilization rates when performing CCOs required the construction of a departure capacity model. It was flexibly constructed, based on the MATLAB software tool, in a number of stages:

(1) The physical constraints were analyzed for variability across departure routes

(2) The different operational constraints were compared to determine which were the most dominant

(3) Preprocess of surveillance data and FDR data to generate database

(4) Databases (actual data) were processed through an additional MATLAB model to determine arrival and departure traffic flows, as well as aircraft type patterns

(5) In parallel, the optimal CCOs were simulated whilst being complied with the identified constraints

(6) The databases (optimized trajectories) were compiled by using the data obtained from the simulations

(7) The databases were processed by the capacity model with the aim of determining the runway utilization rates

The data regarding the considered aircraft types (A330\A319) was processed by the departure capacity model ensuring no loss of separation. The separation values for this calculation were 1000 ft (vertical) and 3 NM (horizontal) [17]. Table 3 presents the evaluated aircraft types per SID.

Table 3: Aircraft types and their associated mass (M) per SID for optimal CCOs and conventional departures.

SID	BARDI2T/CCS1T	BARDI2K/CCS1K
Aircraft (CCO)	M1/M2/M3 (A319)/M1/M2/M3 (A330)	M1/M2/M3 (A330)
Aircraft (conventional)	M1/M2/M3 (A319)/M1/M2/M3/M4 (A330)	M1/M2 (A330)

As it is possible to appreciate on it, the A319 were not considered for BARDI2K/CCS1K taking into account the findings from the surveillance data analysis. It bears out the fact that mediums operating the long leg when departing west are not usual. Regarding the aircraft mass for CCOs, several highly representative take-off mass values were considered where M1 represents the lightest of the studied actual data sample. The figures are not provided in purpose.

Different path lengths, speeds, altitudes, ATC constraints, performance limitations, and operational-cleared levels are some of the numerous parameters, which were considered. The construction of the model was reviewed and discussed with operational staff ensuring the most realistic scenario. The selected mechanism of evaluating the capacity is based on the Monte Carlo simulations that were hand-tailored through MATLAB.

6. Results

Estimating capacity is a matter of paramount importance to all airport planning and analyzing the capacity effects of this particular operational technique on a certain scenario helped on evaluating its potential applicability. The selected method to evaluate CCOs was to study them against actual conventional departures. From an operational point of view, it has been assumed departure separation is based on time. In this regard, a standard time separation of 120 seconds between consecutive departures has been considered. Unfortunately, the combination of certain conventional departures and optimal CCOs may require longer time spacing while ensuring safety operations between the aircrafts along the SIDs.

Figure 3 gathers the information regarding the effects on time spacing in view of the results obtained, is influenced, by the SID and the combination of leading (each represented line) and trailing aircraft (abscissa axis). The following points address those combinations of departures where longer time spacings, than the standard 120 seconds, are required to ensure no loss of separation.

(1) M1B2KA330 (.-+). Being the leading aircraft, an A330 departing BARDI2K/CCS1K whilst performing a conventional departure, it is necessary for an increase of time spacing between 61 and 65 seconds when the trailing aircraft is A319 and between 28 and 38 seconds for A330 performing conventional departures through BARDI2T/CCS1T

(2) M2B2KA330 (-+). Leading aircraft, an A330 departing BARDI2K/CCS1K whilst performing a conventional departure, it is necessary for an increase of time spacing between 52 and 56 seconds when the trailing aircraft is A319 and between 27 and 36 seconds for A330 performing conventional departures through BARDI2T/CCS1T

(3) M1B2KA330 CCO (.-o). Being the leading aircraft, the lightest A330 (M1) departing BARDI2K/CCS1K whilst performing a CCO, it is necessary for an increase of time spacing between 29 and 35 seconds when the trailing aircraft is A319 performing CCOs through BARDI2T/CCS1T and between 7 and 35 seconds for A330 departing through BARDI2T/CCS1T

(4) M2B2KA330 CCO (-o). Being the leading aircraft, the A330 (M2) departing BARDI2K/CCS1K whilst performing a CCO, it is necessary for an increase of time spacing between 25 and 31 seconds when the trailing aircraft is A319 performing CCOs through BARDI2T/CCS1T and between 4 and 31 seconds for A330 departing through BARDI2T/CCS1T

(5) M3B2KA330 CCO (-o). Being the leading aircraft, the heaviest A330 (M3) departing BARDI2K/CCS1K whilst performing a CCO, it is necessary for an increase of time spacing between 22 and 28 seconds when the trailing aircraft is A319 performing CCOs through BARDI2T/CCS1T and up to 28 seconds for A330 departing through BARDI2T/CCS1T

Considering the above factors it is interesting to highlight two findings: first of all, when the leading aircraft is performing a conventional departure via the long leg of the SIDs (BARDI2K/CCS1K), the standard time spacing requires to be increased. This time spacing is likely to be higher when the trailing aircraft type is lighter than the leading one. Secondly, it is interesting to note the fact that when the leading heavy aircraft is performing a CCO via BARDI2K/CCS1K, it is necessary for more time spacing for the trailing aircraft flying CCOs than conventional departures.

6.1. Runway Capacity Effects Due to CCO Expedition. Finally, the effects on capacity for each combination of leading-trailing aircraft were calculated using Monte Carlo simulations. The Monte Carlo simulations were conducted using a hand-tailored model based on MATLAB software tool. Its main objective was to obtain the capacity values per hour of operation considering the previously calculated time spacing between different combinations of aircraft. The simulations were conducted for 10.000

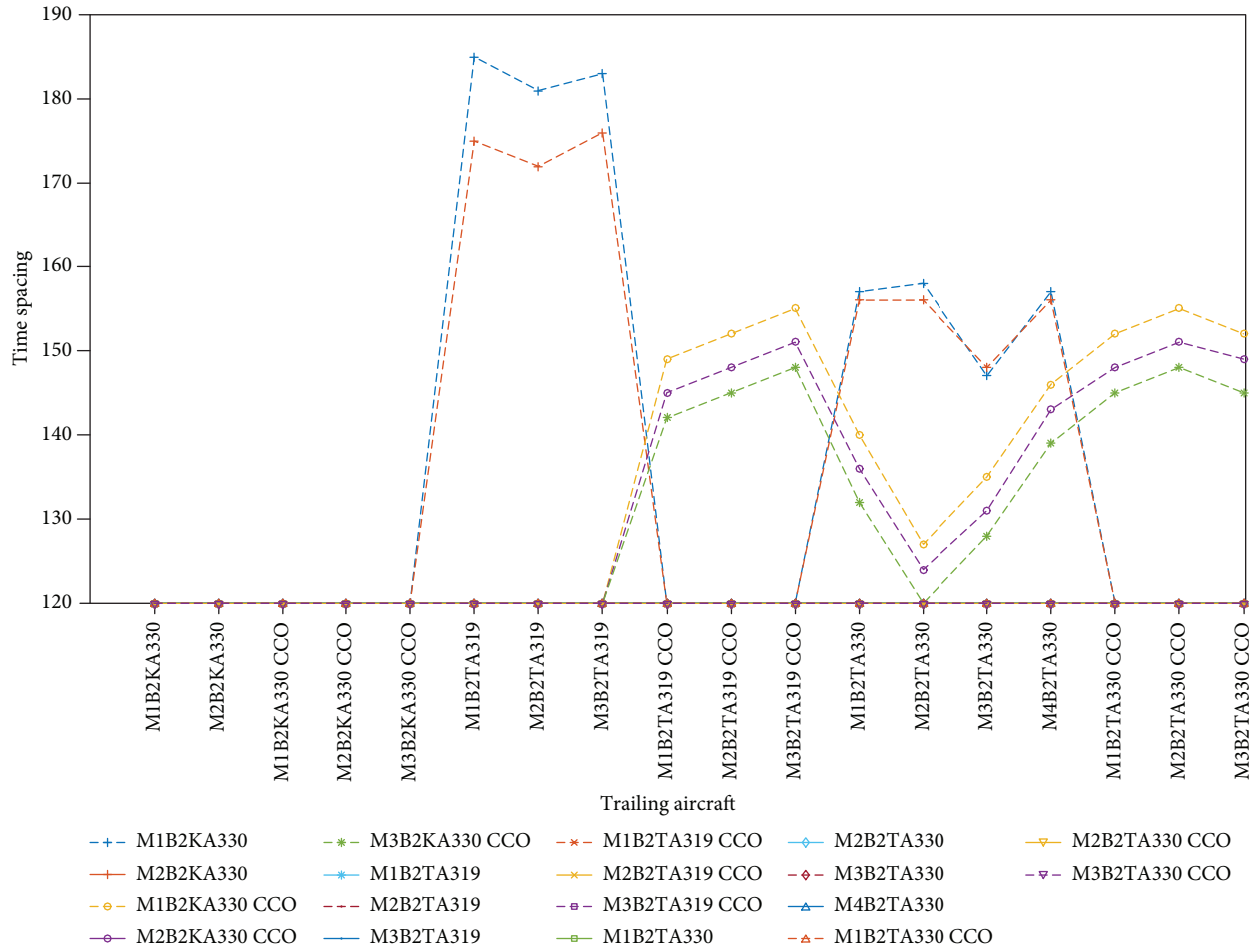

Figure 3: Time separations between aircraft operating BARDI2T/CCS1T and BARDI2K/CCS1K SIDs.

hours per scenario. The model addresses 11 scenarios depending on the percentage of CCOs that covers a total of 110.000 hours analyzed:

(1) *Scenario 1*.100% CCOs

(2) *Scenario 2*. 90% CCOs/10% conventional departures

(3) *Scenario 3*. 80% CCOs/20% conventional departures

(4) *Scenario 4*. 70% CCOs/30% conventional departures

(5) *Scenario 5*. 60% CCOs/40% conventional departures

(6) *Scenario 6*. 50% CCOs/50% conventional departures

(7) *Scenario 7*. 40% CCOs/60% conventional departures

(8) *Scenario 8*. 30% CCOs/70% conventional departures

(9) *Scenario 9*. 20% CCOs/80% conventional departures

(10) *Scenario 10*. 10% CCOs/90% conventional departures

(11) *Scenario 11*. 100% conventional departures

Figure 4 gathers the information regarding the boxplot for each scenario. It allows the reader to appreciate the key results and to identify the key characteristics. The median, which is represented by the line in the box, represents a measure of the center of the data, and the interquartile range box (the green and the red box) brings the distance between the first and the third quartile. Besides, the interquartile range box brings the distance between the first and the third quartile. Last but not the least, the whiskers show the ranges for the bottom 25% and the top 25% of the data values.

(1) *Scenario 1*. The median capacity is 28 movements per hour, and the capacity is as low as 26 and as high as 29. The capacity values are less variable than other scenarios

(2) *Scenario 2*. The median capacity is 28.2 movements. Most of the capacity values are between 28 and 29, and the boxplot manifests top-skewed data, which means that most of the capacity values are lower. The capacity values are as low as 26 and as high as 29

(3) *Scenario 3*. Median capacity value is 28.4, and the interquartile range box is the same as the previous scenario. The boxplot represents top-skewed data. The whisker values are as low as 26 and as high as 29

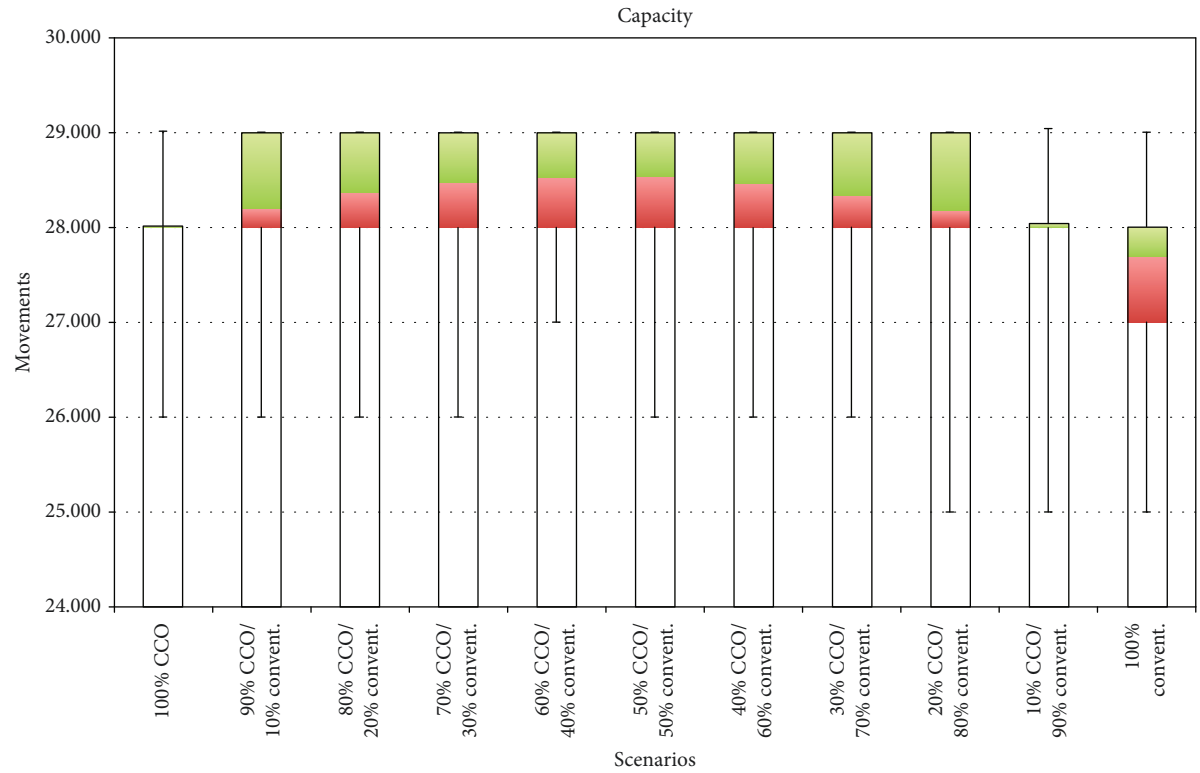

Figure 4: Capacity. Maximum number of aircraft that can be accommodated per hour according to aforementioned scenarios.

(4) *Scenario 4*. The median capacity value is 28.5, and the interquartile range box and the whiskers have the same values on the previous scenario. In this case the main difference is regarding the skewed data, which seems to be slightly top-skewed

(5) *Scenario 5*. The median capacity is 28.5, the interquartile range box remains as before but the bottom whisker increases up to 27. In this case, the data is not skewed

(6) *Scenario 6*. The median capacity is 28.5. The interquartile range box is the same as before, but in this case, the lower whisker goes back to 26. The data distribution is symmetric

(7) *Scenario 7*. Median value is 28.5. Similar to scenario 6 where it is possible to appreciate a change of trend regarding the data which is slightly top-skewed

(8) *Scenario 8*. Median value is 28.3. The main difference compared to scenario 6 is that in this case, it is clearly top-skewed data

(9) *Scenario 9*. Median value is 28.2. In this case, the lower whisker decreases down to 25, and the scenario is clearly top-skewed data

(10) *Scenario 10*. Median capacity value is 28 movements per hour, and the capacity is as low as 25 and as high as 29. The capacity values are less variable than other scenarios

(11) *Scenario 11*. Median capacity value is the lowest, 27.7. The capacity is as low as 25 and as high as 29. Most of the capacity values are between 27 and 28, and the boxplot manifests bottom-skewed data, which means that most of capacity values are higher

Figure 5 reveals that the median values for the studied scenarios vary between 27.7 and 28.5. It is interesting to note the fact that those scenarios where the percentages of each type of traffic are similar, the median presents its highest values. The standard deviation appreciated for the scenarios with lower percentage of CCOs are higher. This indicates that the values are more dispersed.

7. Conclusions

In view of the obtained results, the integration of traffic performing CCOs on departures does not affect negatively in terms of runway capacity. Therefore, it may be argued that whilst the combination between leading-trailing aircraft on mixed departures may affect the capacity, the effect is within an acceptable limit.

The integration of CCO does not necessarily require a specific ATM tool at the controller's working position but the procedures should support them. Nevertheless, the results suggest that integrating CCOs along with a combination of a departure sequence tool tend to mitigate the characteristics of these operating techniques.

Unlike standard arrival routes where aircrafts are tactically guided by air traffic controllers, SID routes tend to follow fixed flight paths. Thus, the optimization of the

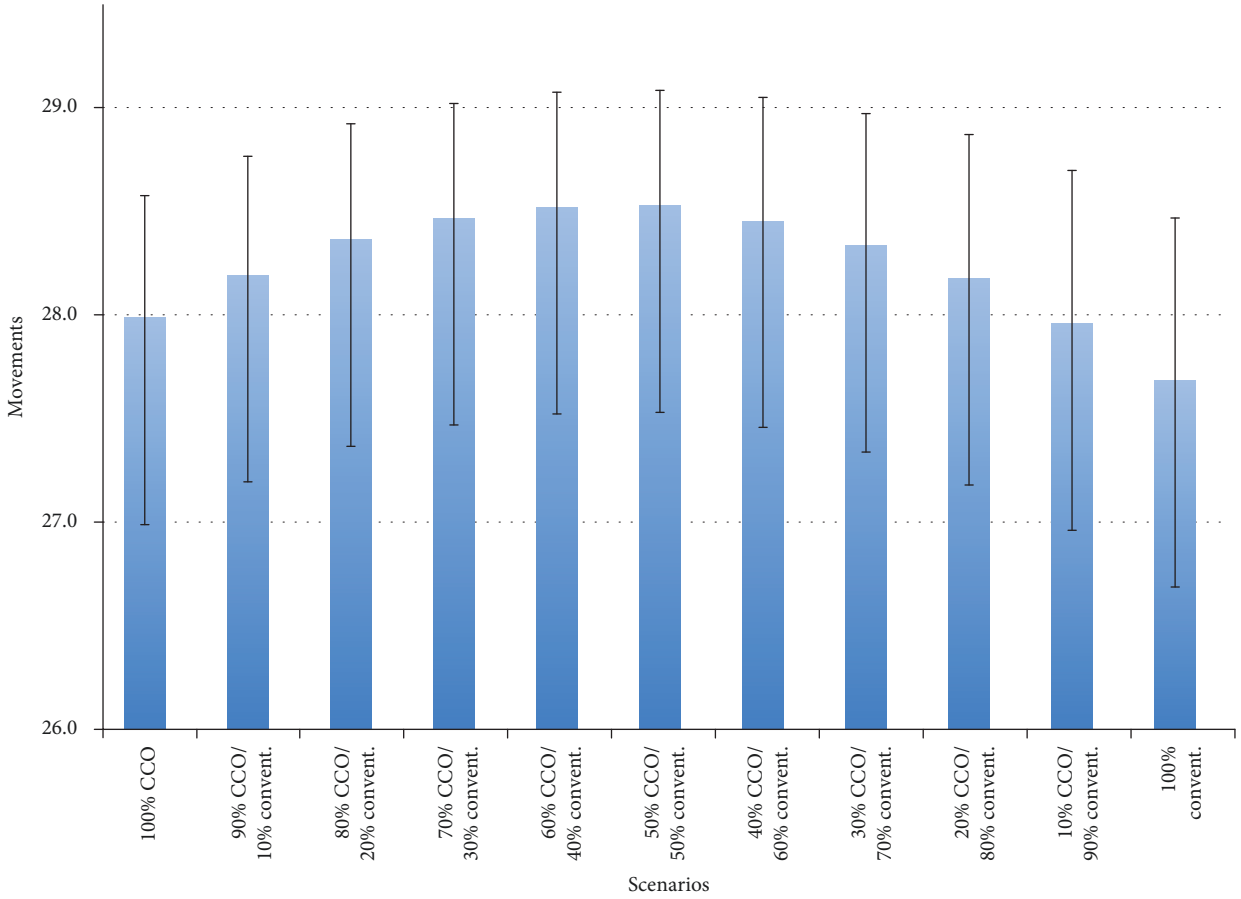

Figure 5: Capacity. Mean capacity values are represented by the bar plot and the associated standard deviations of the sample are illustrated by the whiskers.

vertical profile may be considered an appropriate initiative for departure efficiency.

Allowing the airspace user to fly optimized continuous climb operations will bring significant benefits in greenhouse gas and noise emissions in the vicinity of airports. From the operational point of view, it will lead to more consistent flight paths whilst reducing the number of required radio transmissions. As a consequence, this may be traduced on lower pilot and air traffic controller workload.

This study reinforces the idea of transmitting the importance of CCOs and, furthermore, promotes the usage of this operating technique in TMAs.

Nomenclature

C_d: Coefficient of drag
C_l: Coefficient of lift
D: Drag force
g: Gravity acceleration
h: Altitude
L: Lift force
m: Mass
p: Atmospheric pressure
p_0: Standard value at sea level for atmospheric pressure
t: Time
T: Thrust
V: True airspeed
x: Longitudinal position
η: Thrust-specific fuel flow
γ: Flight path angle
ρ: Atmospheric density
ρ_0: Standard value at sea level for atmospheric density
τ: Temperature
τ_0: Standard value at sea level for temperature.

Data Availability

The data used to support the findings of this study are available from the corresponding author upon request.

Conflicts of Interest

The authors declare that there is no conflict of interest regarding the publication of this paper.

References

[1] ICAO, *Continuous climb operations (CCO) manual*, International Civil Aviation Organization, 1st edition, 2013.

[2] SESAR, "Single sky atm research (2016)," September 2016, http://www.sesarju.eu.

[3] ICAO, *Global air navigation plan 2016-2030*, International Civil Aviation Organization, 2013.

[4] NextGen, "The next generation air transportation system (2016)," https://www.faa.gov/nextgen/.

[5] D. McConnachie, P. Bonnefoy, and A. Belle, "Investigating benefits from continuous climb operating concepts in the national airspace system," in *11th USA Europe Air Traffic Management Research and Development Seminar*, pp. 1–11, Lisbon, Portugal, 2015.

[6] M. Z. Li and M. S. Ryerson, "A data-driven approach to modeling high-density terminal areas: a scenario analysis of the new Beijing, China airspace," *Chinese Journal of Aeronautics*, vol. 30, no. 2, pp. 538–553, 2017.

[7] ICAO, *Manual of the ICAO standard atmosphere*, International Civil Aviation Organization, 3rd edition, 1993.

[8] P. Bonami, A. Olivares, M. Soler, and E. Staffetti, "Multiphase mixed-integer optimal control approach to aircraft trajectory optimization," *Journal of Guidance, Control, and Dynamics*, vol. 36, no. 5, pp. 1267–1277, 2013.

[9] A. Franco and D. Rivas, "Optimization of multiphase aircraft trajectories using hybrid optimal control," *Journal of Guidance, Control, and Dynamics*, vol. 38, no. 3, pp. 452–467, 2015.

[10] D. González-Arribas, M. Soler, and M. Sanjurjo-Rivo, "Robust aircraft trajectory planning under wind uncertainty using optimal control," *Journal of Guidance, Control, and Dynamics*, vol. 41, no. 3, pp. 673–688, 2018.

[11] J. Zhao, R. Zhou, and X. Jin, "Reentry trajectory optimization based on a multistage pseudospectral method," *The Scientific World Journal*, vol. 2014, Article ID 878193, 13 pages, 2014.

[12] F. Fahroo and I. M. Ross, "Direct trajectory optimization by a chebyshev pseudospectral method," *Journal of Guidance, Control, and Dynamics*, vol. 25, no. 1, pp. 160–166, 2002.

[13] J. García-Heras, M. Soler, and F. J. Sáez, "A comparison of optimal control methods for minimum fuel cruise at constant altitude and course with fixed arrival time," *Procedia Engineering*, vol. 80, pp. 231–244, 2014.

[14] AMPL, "AMPL modeling language (2013)," September 2016, http://ampl.com.

[15] Eurocontrol, "User manual for the base of aircraft data (BADA) family 4," in *European organisation for the safety of air navigation*, EUROCONTROL Agency Rue de la Fusee, 2014.

[16] E. R. Boeker, E. Dinges, B. He et al., *Integrated noise model (inm) version 7.0 technical manual, FAA-AEE-08-01 NSN 7540-01-280-550*, U.S. Department of Transportation, Federal Aviation Administration, Office of Environment and Energy, 2008.

[17] ICAO, *PANS-ATM, or procedures for navigation services–air traffic management*, International Civil Aviation Organization, 16th edition, 2016.